

Inhomogeneous multi-carrier superconductivity at $\text{LaXO}_3/\text{SrTiO}_3$ (X=Al or Ti) oxide interfaces

S. Caprara^{1,2}, D. Bucheli¹, N. Scopigno¹, N. Bergeal³, J. Biscaras⁴, S. Hurand³, J. Lesueur³, and M. Grilli^{1,2}

¹*Dipartimento di Fisica Università di Roma Sapienza, piazzale Aldo Moro 5, I-00185 Roma, Italy*

²*ISC-CNR and Consorzio Nazionale Interuniversitario per le Scienze Fisiche della Materia, Unità di Roma Sapienza, Italy*

³*LPEM-UMR8213/CNRS-ESPCI Paris Tech-UPMC, 10 rue Vauquelin, 75005 Paris, France*

⁴*IMPMC-UMR7590/CNRS-UPMC Case 115, 4 Place Jussieu, 75252 Paris, France*

(Dated: February 27, 2015)

Several experiments reveal the inhomogeneous character of the superconducting state that occurs when the carrier density of the two-dimensional electron gas formed at the $\text{LaXO}_3/\text{SrTiO}_3$ (X=Al or Ti) interface is tuned above a threshold value by means of gating. Re-analyzing previous measurements, that highlight the presence of two kinds of carriers, with low and high mobility, we shall provide a description of multi-carrier magneto-transport in an inhomogeneous two-dimensional electron gas, gaining insight into the properties of the physics of the systems under investigation. We shall then show that the measured resistance, superfluid density, and tunneling spectra result from the percolative connection of superconducting “puddles” with randomly distributed critical temperatures, embedded in a weakly localizing metallic matrix. We shall also show that this scenario is consistent with the characteristics of the superconductor-to-metal transition driven by a magnetic field. A multi-carrier description of the superconducting state, within a weak-coupling BCS-like model, will be finally discussed.

PACS numbers: 71.70.Ej, 73.20.-r, 73.43.Nq, 74.81.-g

I. INTRODUCTION

After a two-dimensional electron gas (2DEG) was detected at the interface between two insulating oxides,^{1–4} an increasingly intense theoretical and experimental investigation has been devoted to these systems. The properties of this 2DEG are intriguing within several respects: it can be made superconducting when the carrier density is tuned by means of gate voltage (see Fig. 1), both in $\text{LaAlO}_3/\text{SrTiO}_3$ (henceforth, LAO/STO)^{1,2} and $\text{LaTiO}_3/\text{SrTiO}_3$ (henceforth, LTO/STO)^{3,4} interfaces, thus opening the way to voltage-driven superconducting devices; it exhibits magnetic properties;^{5–10} it displays a strong and tunable^{11,12} Rashba spin-orbit coupling;¹³ it is extremely two-dimensional, having a lateral extension ≈ 5 nm, thereby enhancing the effects of disorder due to extrinsic and/or intrinsic¹² sources.

Magneto-transport experiments reveal the presence of two kinds of carriers in LTO/STO, with high and low mobility, and superconductivity seems definitely to develop as soon as high-mobility carriers appear,^{4,14} when the carrier density is tuned above a threshold value, by means of gate voltage V_g . When the temperature T is lowered, the electrical resistance is reduced, and signatures of a superconducting fraction are seen well above the temperature at which the global zero resistance state is reached (if ever). The superconducting fraction decreases with decreasing V_g , although a superconducting fraction survives at values of V_g such that the resistance stays finite down to lowest measured temperatures. When V_g is further reduced, the superconducting fraction eventually disappears, and the 2DEG stays metallic at all temperatures, seemingly undergoing weak localization at low T . At yet smaller car-

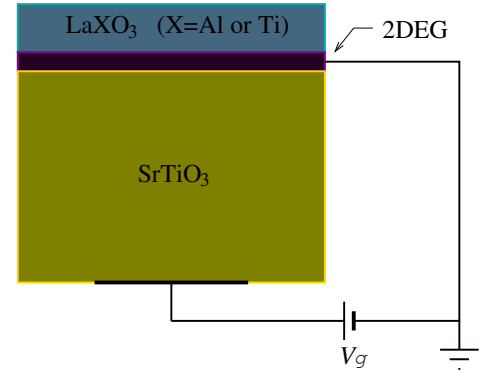


FIG. 1. Scheme of an oxide interface (not in scale), in the back gating configuration. The LAO (or LTO) topmost slab has a thickness of few nm, whereas the STO slab is ≈ 0.5 mm thick. The back gate voltage V_g is employed to tune the carrier density of the 2DEG. The top gating configuration is also possible.

rier densities, the system behaves as an insulator. The width of the superconducting transition is anomalously large and cannot be accounted for by reasonable superconducting fluctuations.¹⁵ This phenomenology suggests instead that an inhomogeneous 2DEG is formed at these oxide interfaces, consisting of superconducting “puddles” embedded in a (weakly localizing) metallic background, opening the way to a percolative superconducting transition.¹⁶ Inhomogeneities are revealed in various magnetic experiments,^{5–7,10} in tunneling spectra,¹⁷ and in piezoforce microscopy measurements.¹⁸ Seemingly, inhomogeneities at the nanometric scale coexist with larger (e.g., micrometric) scale inhomogeneities, revealed by the occurrence of striped textures in the current

distribution¹⁹ and in the surface potential.²⁰

Various aspects of the phenomenology of oxide interfaces (henceforth referred to as LXO/STO interfaces, when referring to both LAO/STO and LTO/STO) have been separately discussed before.^{4,12,15,16,21,22} Here, we first provide new compelling evidence of the inhomogeneous character of the 2DEG, extending previous multi-carrier analyses of magneto-transport measurements to deal with inhomogeneous systems. We then put together the various pieces of the jigsaw into an overall coherent theoretical framework.

The plan of the present piece of work is the following. In Sec. II, we propose a model for multi-carrier magneto-transport in inhomogeneous systems, and show that previous analyses of the magnetoresistance and Hall resistance measurements in terms of two different species of carriers⁴ is fully consistent with the inhomogeneous character of the 2DEG at LAO/STO and LTO/STO interfaces. In Secs. III, IV, and V, we revisit some of our previous results. Assuming inhomogeneity as an empirical evidence, we show that resistance measurements⁴ and the topographic mapping of the superfluid density¹⁰ can be accounted for within a percolative scheme. In Sec. VI, we discuss some preliminary aspects of a theory for metal-insulator-superconductor tunneling in inhomogeneous superconductors that is apt to reproduce the measured tunneling spectra.²³ In Sec. VII, we provide further evidence for inhomogeneous superconductivity at oxide interfaces, coming from the peculiar multiple quantum critical scaling, observed when superconductivity is suppressed by means of a magnetic field, revisiting the results of Ref. [21]. In Sec. VIII, relying on the results of Ref. [22], we show that the properties of the superconducting puddles (e.g., their fraction, and critical temperatures) can be extracted from experiments and used to model intra-puddle multi-carrier superconductivity, gaining insight about the pairing mechanism. Although some features of the diamagnetic response are seemingly related to strong superconducting coupling,¹⁰ we show that inhomogeneities and multi-carrier superconductivity fully account for the behavior of these systems within a standard weak coupling BCS scheme. Concluding remarks are found in Sec. IX.

II. MULTI-CARRIER MAGNETO-TRANSPORT IN INHOMOGENEOUS SYSTEMS

The detection of two species of carriers, with high and low mobility, by means of magneto-transport measurements in LTO/STO,⁴ is not necessarily a direct evidence of inhomogeneity, since the two species could coexist in a homogeneous manner. However, to account for the phenomenology of the superconducting state of the 2DEG at LXO/STO interface, we proposed that the 2DEG is inhomogeneous, with higher density regions (the superconducting puddles) and lower density regions (the metallic background).^{21,22} Assigning a band structure to the

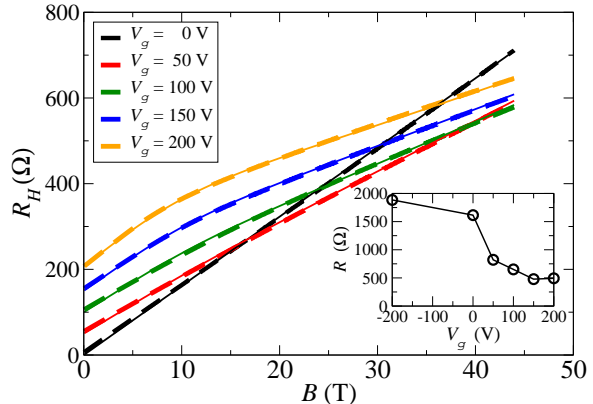


FIG. 2. Hall resistance as a function of magnetic field for different gate voltages V_g , measured at $T = 4.2$ K in a LTO/STO 15-unit-cell thick sample (sample A of Ref. [4]). Solid lines correspond to experimental data, taken from Ref. [4], while the dashed lines are obtained here, fitting the data with Eq. (2). For clarity, the curves have been shifted upwards by $50\,\Omega$ in increasing voltage order. Inset: Sheet resistance R , obtained via Eq. (1), as a function of the gate voltage.

system, one is then led to assume that, when the density is large enough to fill the bands occupied by the high-mobility carriers, these should locally coexist with low-mobility carriers occupying the lower-lying levels (see also Sec. VIII). A picture then emerges in which the low-mobility carriers alone are present in the metallic background, whereas they coexist with the high-mobility carriers in the superconducting puddles. To improve our description of LXO/STO interfaces, we must then rely on a theory for multi-carrier magneto-transport that is apt to deal with an inhomogeneous system. One such theory has been developed in the form of an Effective Medium Theory (EMT) for the Hall conductance of a binary medium resulting from the mixture of two phases, based on rotation transformations (see Ref. [24] for a detailed description of this method).

In our description of the LXO/STO interfaces, one (less dense) phase hosts one species of carriers, with low mobility, and the other (denser) phase hosts two species of carriers, with low and high mobility. Following Ref. [24], we first define the conductivity tensor for each of the two coexisting phases, in the presence of a magnetic field of amplitude B . The diagonal elements of the conductivity tensor are

$$\sigma_{xx}^{(1)}(B) = \frac{\sigma_1}{1 + [\beta_1(B)]^2},$$

$$\sigma_{xx}^{(2)}(B) = \frac{\sigma_1}{1 + [\beta_1(B)]^2} + \frac{\sigma_2}{1 + [\beta_2(B)]^2},$$

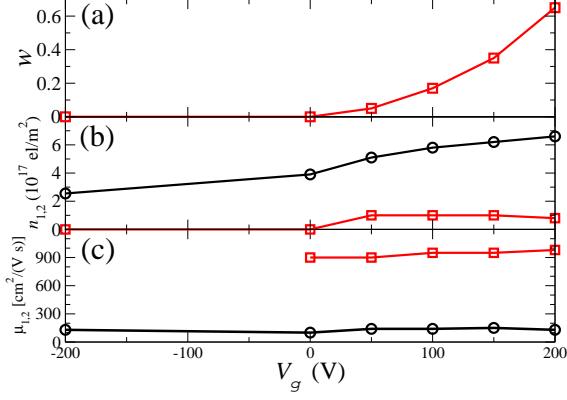


FIG. 3. (a) Fraction w of the high-mobility metallic phase [phase (2), see text]; (b) Densities of the less (n_1 , empty circles) and more (n_2 , empty squares) mobile carriers extracted from the fits of the Hall resistance, Eq. (2), as a function of gate voltage measured at $T = 4.2$ K. (c) Mobilities μ_1 (empty circles) and μ_2 (empty squares) of the majority (low-mobility) and minority (high-mobility) carriers, respectively, extracted from Eq. (2). Type 1 (low-mobility) carriers only are present in the phase (1), while both type 1 and type 2 (high-mobility) carriers are present in the phase (2).

and the off-diagonal elements are

$$\sigma_{xy}^{(1)}(B) = \frac{\sigma_1 \beta_1(B)}{1 + [\beta_1(B)]^2},$$

$$\sigma_{xy}^{(2)}(B) = \frac{\sigma_1 \beta_1(B)}{1 + [\beta_1(B)]^2} + \frac{\sigma_2 \beta_2(B)}{1 + [\beta_2(B)]^2}.$$

$$\sigma_{xy}^{EMT}(B, \epsilon) = \left\{ \frac{[\sigma_{xx}^{EMT}(B, \epsilon) + \sigma_{xx}^{EMT}(B, -\epsilon)] [\sigma_{xx}^{(1)}(B) \sigma_{xy}^{(2)}(B) + \sigma_{xy}^{(1)}(B) \sigma_{xx}^{(2)}(B)]}{\sigma_{xx}^{(1)}(B) + \sigma_{xx}^{(2)}(B)} \right. \\ \left. - \frac{[\sigma_{xx}^{EMT}(B, \epsilon) - \sigma_{xx}^{EMT}(B, -\epsilon)] [\sigma_{xx}^{(1)}(B) \sigma_{xy}^{(2)}(B) - \sigma_{xy}^{(1)}(B) \sigma_{xx}^{(2)}(B)]}{\sigma_{xx}^{(1)}(B) - \sigma_{xx}^{(2)}(B)} \right\} \frac{1}{2\sigma_{xx}^{EMT}(B, -\epsilon)}.$$

From the above relations, the expression for the Hall resistance of the inhomogeneous system can finally be derived,

$$R_H^{EMT}(B, \epsilon) = \frac{\sigma_{xy}^{EMT}(B, \epsilon)}{[\sigma_{xy}^{EMT}(B, \epsilon)]^2 + [\sigma_{xx}^{EMT}(B, \epsilon)]^2}, \quad (2)$$

which we used to accurately fit the experimental Hall resistivity data of LTO/STO,⁴ under strong magnetic field and at different gate voltages (see Fig. 2). This procedure allows to extract the values of the mobilities μ_i and of the densities n_i of the two species of carriers, as well as the fraction of the system occupied by the su-

perconducting puddles, w . These values are reported in Fig. 3, while the inset of Fig. 2 displays the evolution of the normal-state sheet resistance, extracted via Eq. (1) as $R = [\sigma_{xx}^{EMT}(B = 0, \epsilon)]^{-1}$, with changing V_g .

Hereafter, the superscripts (1) and (2) label the two phases, the subscripts 1 and 2 label the two species of carriers (with low and high mobility, respectively), and we adopt the notations $\beta_i(B) \equiv \mu_i B/c$ and $\sigma_i \equiv en_i \mu_i$, where n_i is the carrier density and μ_i is the mobility of the i -th species of carriers. We point out that the peculiar aspect of our present description is that both species of carriers contribute in parallel to the conductivity tensor in the phase (2), which we identify with the higher density superconducting puddles. We indicate with $w \equiv \frac{1}{2} - \epsilon$ the fraction of the system occupied by the superconducting puddles, ϵ being the deviation from the percolation threshold, that changes sign when the minority phase ($w < \frac{1}{2}$, $\epsilon > 0$) percolates and becomes the majority phase ($w > \frac{1}{2}$, $\epsilon < 0$), the threshold being $w = \frac{1}{2}$ in two-dimensional systems.

Within EMT, the diagonal element of the conductivity tensor of the inhomogeneous (two-phase) system can be found, that correctly reproduces the limiting case of a pure phase, and takes the form²⁴

$$\sigma_{xx}^{EMT}(B, \epsilon) = \epsilon \left[\sigma_{xx}^{(2)}(B) - \sigma_{xx}^{(1)}(B) \right] + \sqrt{\epsilon^2 \left[\sigma_{xx}^{(1)}(B) - \sigma_{xx}^{(2)}(B) \right]^2 + \sigma_{xx}^{(1)}(B) \sigma_{xx}^{(2)}(B)}. \quad (1)$$

Then, exploiting duality relations that connect the various elements of the conductivity tensor when the minority and majority phases are interchanged (see Ref. 24), one obtains the EMT expression for the off-diagonal element of the conductivity tensor of the inhomogeneous (two-phase) system

perconducting puddles, w . These values are reported in Fig. 3, while the inset of Fig. 2 displays the evolution of the normal-state sheet resistance, extracted via Eq. (1) as $R = [\sigma_{xx}^{EMT}(B = 0, \epsilon)]^{-1}$, with changing V_g .

Our present findings cast in a somewhat different perspective the analysis carried out in Ref. [4], where the appearance of more mobile carriers around $V_g = 0$ V was found. While on the one hand we fully confirm that result, on the other hand we find here that the magneto-transport data are well described assuming that these carriers do not appear uniformly in the whole system. Rather high- and low-mobility carriers coexist in a high-

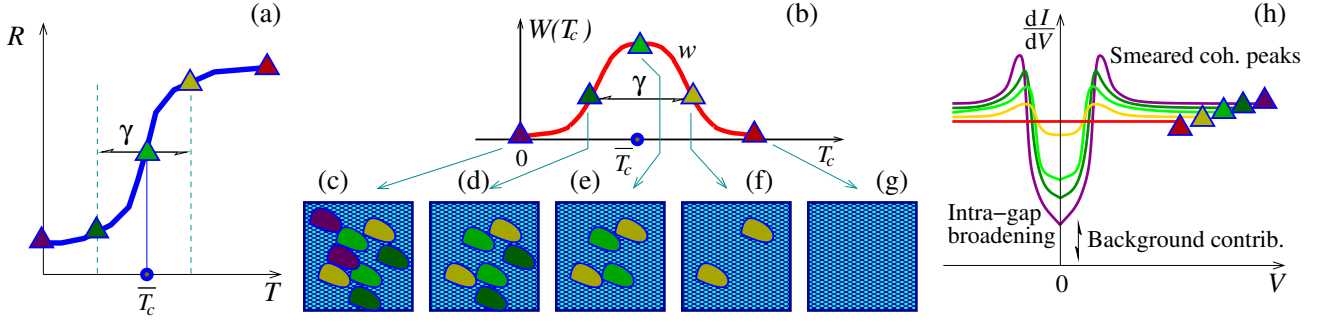


FIG. 4. (a) Sketch of the behavior of the resistance as a function of temperature in a case when the superconducting fraction does not percolate. (b) Distribution of critical temperatures $W(T_c)$ in the superconducting puddles, that occupy a fraction w of the sample (the remaining $1 - w$ fraction will never become superconducting). (c–g) When the temperature is reduced [from (g) to (c)] superconducting puddles appear in the system as soon as the local critical temperature exceeds T . However, if the puddles do not percolate down to $T = 0$, the global zero resistance state is never reached. (h) Sketch of the tunneling spectra measured in LAO/STO, as a function of bias voltage V : At temperatures well above the temperature at which the zero resistance state is reached (if ever), a suppression is observed in the tunneling spectra around zero bias, accompanied by more or less pronounced coherence peaks above the gap. The coherence peaks are smeared and the intra-gap spectra are broadened, with non-vanishing zero bias spectral weight, that we attribute to the metallic background. The curves are labelled by colored triangles that refer to the corresponding temperatures in panel (a).

mobility metallic phase, here identified with the phase (2), which is inhomogeneously distributed at the interface and spatially separated from the less metallic phase (1), where only one species of less mobile carriers is present. In this framework, the enhanced conductivity around $V_g = 0$ V and the changes of slope of the Hall resistance at high magnetic field occur because a finite fraction w of phase (2), characterized by an overall higher carrier density and hosting high-mobility carriers, appears around this gate voltage [see Fig. 3(a)]. In agreement with the conclusions of Ref. [4], we also find that the more mobile carriers have a lower density than the low-mobility ones [Fig. 3(b)] but, at odds with the results obtained within a homogeneous description, in the present inhomogeneous scheme the mobilities of the two species stay rather constant over the whole range of gate voltages [see Fig. 3(c)].

III. PERCOLATIVE SUPERCONDUCTIVITY

After assessing the occurrence of inhomogeneous multi-carrier magneto-transport at LZO/STO interfaces, we discuss the superconducting transition that is driven by tuning the gate voltage V_g (i.e., the carrier density) above a threshold value. It has been shown that the superconducting transition occurring in inhomogeneous systems is well described within the EMT.¹⁵ EMT is a mean-field-like theory apt to describe a random resistor network (RRN) that lacks spatial correlations. The EMT equations are obtained embedding one given random resistance R_i in an effective medium of constant resistance R . This latter is chosen in such a way as to have the same current flowing through R_i as in the RRN. The EMT resistance can be shown¹⁵ to be larger than the parallel and smaller than the series of the random resistances,

the two limiting values being reached in infinite and one dimensions, respectively.

The resistance of the LTO/STO interface exhibits a marked suppression due to incipient superconductivity, that is accurately fitted²² assuming that the superconducting puddles occupy a fraction $w < 1$ of the sample, and that each puddle is characterized by a random local critical temperature T_c . For the sake of definiteness, we adopt a Gaussian distribution of critical temperatures, $W(T_c)$, parametrized by its mean value \bar{T}_c and its width γ . The remaining $1 - w$ fraction of the sample is occupied by the metallic background. The resistance at temperature T is found within EMT to be^{15,16,22}

$$R(T) = R_\infty \left[(1 - w) + w \operatorname{erf} \left(\frac{T - \bar{T}_c}{\gamma\sqrt{2}} \right) \right],$$

and results form the metallic background (first term inside the square brackets) and from not yet superconducting puddles (i.e., those puddles with $T_c < T$, second term inside the square brackets, erf being the error function); the remaining puddles (i.e., those with $T_c > T$), have become superconducting and do not contribute to the resistance. The high-temperature resistance R_∞ , w , \bar{T}_c , and γ are used as fitting parameters. The global zero resistance state is reached at the percolative transition temperature $T_p \leq \bar{T}_c$ such that

$$\operatorname{erf} \left(\frac{T_p - \bar{T}_c}{\gamma\sqrt{2}} \right) = \frac{w - 1}{w}. \quad (3)$$

A solution for T_p only exists if the superconducting fraction of the 2DEG can percolate in the two-dimensional system, i.e., for $w \geq \frac{1}{2}$. When $T_p < 0$, or when it is not at all defined (for $w < \frac{1}{2}$), the resistance remains finite down to $T = 0$, although the presence of a sizable (yet

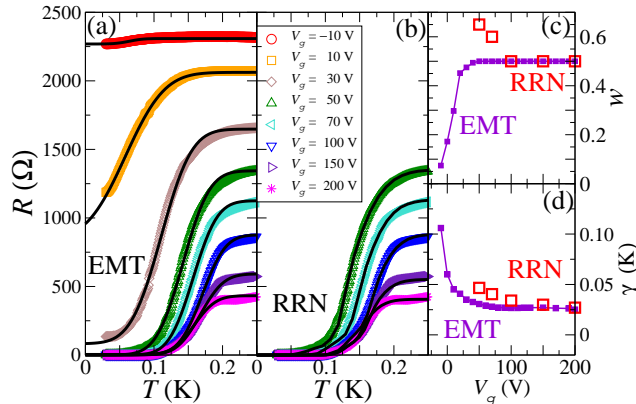


FIG. 5. (a) Measured sheet resistance in a LAO/STO sample, for $V_g = -10, 10, 30, 50, 70, 100, 150, 200$ V. The solid lines are the EMT fits. (b) Same as in panel (a), with fewer experimental curves, fitted by RRN curves (solid lines). (c) Weight of the superconducting fraction and (d) width of the T_c distribution, from EMT (line and small filled squares) and RRN (large open squares) fits.

not percolating) superconducting fraction is mirrored by a sizable suppression of $R(T)$, as sketched in Fig. 4(a).

The resistances measured in a LTO/STO sample as a function of T for various values of the gate voltages V_g ,⁴ are shown in Fig. 5(a) together with the fitting EMT curves (symbols and solid lines, respectively). Fig. 5 is inspired to a similar figure of Ref. [22], with new elements included to make explicit contact with the overview contained in this piece of work. The set of parameters $R_\infty, w, \bar{T}_c, \gamma$, i.e., the distribution of the puddles, changes with changing the carrier density by means of gating.

We are thus able to extract from the fits the mean intra-puddle critical temperature \bar{T}_c [i.e., the temperature at which $R(T)$ changes curvature within EMT], which will be analyzed in Sec. VIII, and the overall superconducting fraction w , tracked by the solid line with filled squares in Fig. 5(c). We point out that EMT disregards spatial correlations, so that the presence of pronounced tails in the resistance, in the presence of a percolating superconducting cluster, force the overall superconducting fraction to be¹⁵ $w \approx \frac{1}{2}$, as shown in Fig. 5(c). The width γ of the Gaussian distribution of T_c is plotted as a solid line with filled squares Fig. 5(d). It increases as the fraction w of the puddles goes to zero. This is rather natural because a reduction of the carrier density is expected to emphasize the effects of disorder, so that fluctuations of the local superconducting critical temperature should increase, leading to a broadening of the T_c distribution.

A comment is now in order. Dealing with superconducting puddles embedded in a metallic background, we expect the proximity effect²⁵ to play an important role in LTO/STO interfaces. Within EMT, this effect sure entails a temperature dependence of the superconducting

fraction w . However, when fitting the resistance curves $R(T)$, the introduction of a temperature dependent $w(T)$ is not viable, because it would made a good fit by definition. Nonetheless, the role of proximity effect can be analyzed when discussing tunneling spectra. We shall come back to this point in Sec. VI.

IV. SUPERFLUID DENSITY IN INHOMOGENEOUS SUPERCONDUCTORS

The inhomogeneous character of the 2DEG at the LXO/STO interfaces raises the question of the description of the superfluid properties in a mixture of two phases. The superfluid density n_s was measured¹⁰ by means of a SQUID in LAO/STO interfaces. The measurements average over micrometric scales and are therefore not sensitive to submicrometric inhomogeneities. Nonetheless, the idea that the 2DEG at these interfaces is inhomogeneous, is still supported by the evidence of variations of n_s on the micrometric scale within a given sample. Encouraged by the marked similarity of the resistance curves in LAO/STO and in LTO/STO, we apply EMT also to describe the measured local n_s as an average over an inhomogeneous state of submicrometric puddles. We point out that recent experiments in LTO/STO²¹ led to estimate the typical size of the puddles to be ≈ 100 nm, thereby supporting this idea.

We proceeded extending EMT to small frequency ω ,²² and assigning to the metallic background a Drude-like complex conductivity $\sigma_M(\omega) = \Lambda(\Gamma + i\omega)^{-1}$ and to the superconducting puddles a purely reactive conductivity $\sigma_S(\omega) = \Lambda(i\omega)^{-1}$. We then defined the resistivity $\rho_S(\omega) \equiv \sigma_S^{-1}(\omega)$ and $\rho_M(\omega) \equiv \sigma_M^{-1}(\omega) = \rho_0 + \rho_S(\omega)$, with $\rho_0 \equiv \Gamma/\Lambda$. At high T , the system is metallic and $\rho(\omega) = \rho_M(\omega)$. However, when the temperature is lowered, the static resistivity vanishes within each individual puddle as soon as T equals the local T_c . Although the full expression of the complex resistivity can be found within EMT, aiming at describing the static diamagnetic response, we give only the expression up to terms $\sim \omega$, i.e., $\rho(\omega) \approx \rho_0(w_M - w_S)\vartheta(w_M - w_S) + |w_M - w_S|^{-1}\rho_S(\omega)$, where ϑ is the Heaviside function, w_S is the fraction of puddles that have become superconducting (at a given temperature), and $w_M = 1 - w_S$ is the non superconducting fraction (resulting both from puddles that have not yet become superconducting and from the metallic background). Evidently, when $w_M > w_S$, the conductivity is Drude-like. However, below the percolation temperature T_p (whenever defined), $w_M < w_S$, and the conductivity is purely reactive $\sigma(\omega) = \Gamma(w_S - w_M)(i\omega)^{-1}$. Therefore, employing also Eq. (3), we find that the superfluid density of the percolating two-dimensional network for $T \leq T_p$ is

$$n_s \propto w_S - w_M \\ = w \left[\text{erf} \left(\frac{T_p - \bar{T}_c}{\gamma\sqrt{2}} \right) - \text{erf} \left(\frac{T - \bar{T}_c}{\gamma\sqrt{2}} \right) \right]. \quad (4)$$

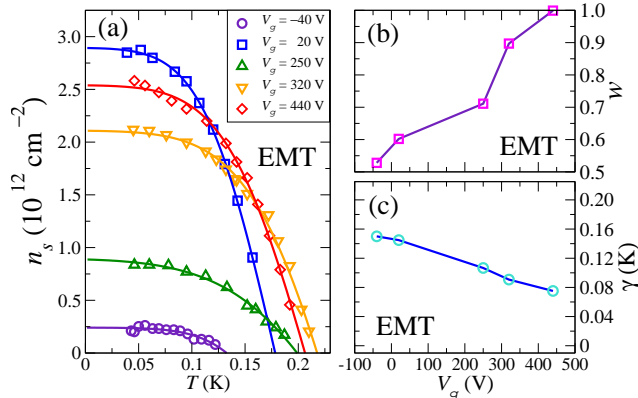


FIG. 6. (a) Superfluid density (symbols) as a function of T and EMT fits according to Eq. (4) (solid lines). Weight of the superconducting fraction (b) and width of the T_c distribution (c) extracted from the EMT fits, as a function of V_g . The lines are guides to the eye.

In Fig. 6(a), this average superfluid density and our EMT fits [Eq. (4)] are reported, for different values of V_g . Fig. 6 is inspired to a similar figure of Ref. [22], again suitably modified to make explicit contact with the present discussion. The behavior of $n_s(T)$, although qualitatively resembling the BCS prediction, may quantitatively differ from it. The slope at $T = T_p$, for instance, is controlled by the width γ of the distribution $W(T_c)$. Thus, the deviations from standard BCS prediction measured in Ref. [10], and attributed to a tendency to strong coupling, are here alternatively explained claiming that the 2DEG is in a weak coupling BCS regime (see Sec. VIII), but the superfluid density is intrinsically inhomogeneous at the submicrometric scale and is averaged at the micron scale by the SQUID pick-up loop used in Ref. [10]. We point out that our mean field approach is justified by the observation that the channels down to 500 nm wide share properties similar to those of the larger samples.²⁶ Our fits yield the fraction w of volume occupied by the puddles, extracted from measurements of the superfluid density and reported in Fig. 6(b). It ranges from $\frac{1}{2}$ to 1, and is always larger than the fraction obtained from transport measurements. This is not surprising, because transport mainly probes the long-range connectivity of the percolating path, regardless of dead ends and disconnected superconducting regions,²⁷ whereas diamagnetic screening measurements are sensitive to all sufficiently large superconducting loops, even when not connected to the backbone. In this case, the diamagnetic fraction can be large, while the long-distance connectivity is small, if many puddles or loops are disconnected (see Sec. V). Fig. 6(c) reports the behavior of the width γ of the distribution $W(T_c)$, inferred from the superfluid density. We point out that, despite the fact that we are dealing with different materials and physical quantities, the behavior

of γ resembles that obtained from transport in LTO/STO [Fig. 5(d)] and is of comparable magnitude.

Of course, a proof of the above arguments requires a model accounting for space correlations, that includes both closed loops (relevant for diamagnetism) and connected paths (relevant for transport). While such a model has been found for transport (see Sec. V), a similar model for the diamagnetic response is not yet available, so our discussion on this specific aspect has a purely speculative character. An experimental test to our scenario could be provided by the observation of different diamagnetic responses in field-cooled and zero-field-cooled samples. In the first case one expects substantially smaller diamagnetic fraction, since a sizable flux would be trapped in the normal part encircled by the superconducting loops (see the shaded region in Fig. 7 and the discussion in Sec. V).

The study of the dynamical response of an inhomogeneous superconductor at finite frequency, within EMT, is presently under investigation. A somewhat similar approach, applied to superconducting stripes in high-temperature superconductors, can be found in Ref. [28].

V. SPACE CORRELATIONS WITHIN THE SUPERCONDUCTING CLUSTER

A possible explanation for the discrepancy between the superconducting fraction w observed in transport and diamagnetism measurements may rest upon the filamentary structure of the superconducting cluster at oxide interfaces.²² So far, we have made use of the mean-field-like EMT, which completely neglects spatial correlations. To investigate the mechanisms determining the superconducting fraction observed in transport, $w \approx \frac{1}{2}$, we solved a RRN where the superconducting puddles form a spatially correlated cluster embedded in a metallic matrix. Preliminary results¹⁶ indicated that a superconducting cluster which is dense at short distances and filamentary at larger distances is necessary in order to reproduce the observed tails of the resistance curves near percolation.

To this purpose, we generated a fractal-like cluster with small long-scale connectivity, that percolates only when almost all bonds have become superconducting. We point out that the fractality of the clusters is an artifice to produce spatially correlated networks that are at the same time dense at short distances and filamentary over long distances. For a Gaussian $W(T_c)$, the low temperature tail of the distribution must be necessarily reached, and a correspondingly pronounced tail in the resistance is obtained. Compact clusters fail to reproduce the tails in the resistance, in the absence of filamentary structures over long distances. Our systematic investigation showed that the presence of loosely connected filaments is a necessary ingredient to reproduce the behavior of $R(T)$ near percolation. On the other hand, a purely filamentary structure, no matter how dense at short distance, is too loose and is not apt to describe the behavior of

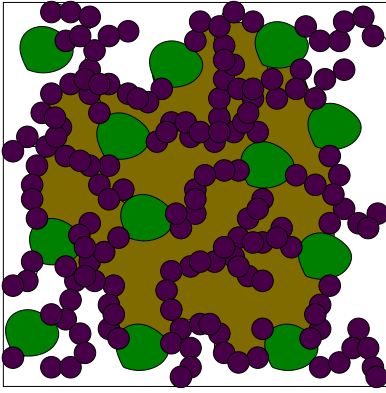


FIG. 7. Sketch of the RRN with superpuddles (green regions) connected by filaments of puddles (purple circles). The large shaded region, that does not contribute to superconducting transport, contributes instead to the diamagnetic response in the case of a zero-field-cooling measurement, since the superconducting currents confined in the superpuddles and loop structures encircled by the puddles are apt to screen a magnetic field. In the case of a field-cooling measurement, one expects instead that the magnetic flux is frozen within the loop structures encircled by the puddles.

$R(T)$ at higher temperatures. In order to tune the density of the superconducting cluster without significantly changing the long-distance connectivity, we decorate the filaments with randomly distributed superpuddles, for simplicity assumed circular, their number and size being chosen to produce weights w ranging from 0.3 to 0.7 (see the sketch in Fig. 7). Superpuddles may be produced by large tails in the distribution of the puddle sizes, or by extrinsic pinning centers, promoting the nucleation of much larger puddles. We systematically investigated the effect of the size and density of the superpuddles. A smaller fraction of larger superpuddles or a larger fraction of smaller superpuddles are essentially equivalent, as long as the superpuddles do not overlap to form percolating clusters.

In Fig. 5(b), we show our fits of the resistance obtained within our RRNs. Noticeably, even though the superconducting fraction w is no longer forced to $\frac{1}{2}$, as it was instead within EMT, the resistance displays pronounced tails only if $0.50 \lesssim w \lesssim 0.65$. The lower bound is imposed by the high slope at intermediate temperatures whereas the upper bound is due to the pronounced tail near percolation. In Figs. 5(c) and (d) we show the fraction w occupied by the superconducting cluster and the width γ of the Gaussian distribution $W(T_c)$ obtained within the RRN (open circles): γ qualitatively resembles the width obtained within EMT, and increases upon lowering V_g . Thus, EMT and RRN models lead to similar results about the distribution of T_c and its variation with V_g , provided the RRN is dense at short distances and filamentary over long distances.

VI. TUNNELING SPECTRA OF INHOMOGENEOUS SUPERCONDUCTORS

Another possibility of probing the inhomogeneous character of the superconducting state at LXO/STO interfaces is provided by tunneling experiments. Recent metal-insulator-superconductor tunnel spectroscopy measurements on LAO/STO,²³ reveal the occurrence of a state with finite resistance, but superconducting-like density of states (DOS). The measurements are performed depositing a metallic Au electrode on top of the insulating LAO layer, and applying a bias voltage V to drive a tunnel current I between the electrode and the 2DEG. The electrode measures several hundreds μm across, thus being orders of magnitude larger than the nanoscale inhomogeneities.²¹ At the lowest measured temperature, $T = 30$ mK, the spectra reveal a gap in the DOS at the Fermi energy, over the entire range of explored gate voltages $V_g \in [-300, 300]$ V, accompanied by more or less broadened coherence peaks above the gap, pointing to superconducting coherence and pairing as the origin of DOS suppression [see Fig. 4(h)]. In the carrier depleted regime ($V_g \ll 0$), the suppression is found even in the absence of global superconductivity, again highlighting the inhomogeneous character of the state formed by superconducting puddles embedded in a metallic matrix. At very low carrier concentration, $V_g \approx -300$ V, the coherence peaks have been completely smeared, although a sizable gap is still present as a signature of (incoherent) pairing. We shall call pseudo-gap state a state displaying at the same time a DOS suppression in the tunneling spectra, accompanied by more or less pronounced coherence peaks, and non-zero electrical resistance. At higher carrier concentration, $V_g = 200$ V, the 2DEG displays a superconducting gap and coherence peaks that decrease with increasing temperature and vanish around 300 mK (which agrees with the critical temperature of bulk STO reported in Ref. [29]). At $V_g \leq 0$, the gap closes and the coherence peaks vanish, at temperatures much higher than the global T_c .

Since, as it was observed above, the tunneling spectra are taken over a spot measuring several hundreds μm across, we proposed³⁰ that the observed pseudo-gap results from an average over superconducting regions (the superconducting puddles, with a DOS described by standard BCS theory) and metallic regions (composed of the metallic background and of not yet superconducting puddles) with constant DOS N_0 .

The differential conductance is usually written as

$$\frac{dI}{dV}(V) = G_0 - G_1 \int_{-\infty}^{\infty} f'(E + eV) N(E) dE, \quad (5)$$

where $N(E)$ is the DOS, $f'(E)$ is the derivative of the Fermi distribution function, the positive constant G_0 customarily accounts for effects such as leakage currents, and G_1 is a dimensional constant. We recall that in our model superconducting pairing occurs within each puddle below

a local critical temperature T_c , randomly distributed according to a probability distribution $W(T_c)$. The DOS of the 2DEG probed in tunneling spectra has three distinct contributions,

$$N(E) = (1 - w)N_0 + wN_0 \int_{-\infty}^T dT_c W(T_c) + w \int_T^{\infty} dT_c W(T_c) N_{\Delta(T_c, T)}(E). \quad (6)$$

The first two terms correspond to the metallic background and to puddles where pairing has not taken place yet, respectively, and fully account for the zero bias background observed in the tunneling spectra, allowing us to take $G_0 = 0$ in Eq.(5). The third term corresponds to puddles that developed a finite pairing gap Δ . The DOS within these puddles is taken as

$$N_{\Delta}(E) = \left[(1 - x) \frac{|E|}{\sqrt{E^2 - \Delta^2}} + x \right] N_0 \vartheta(|E| - \Delta).$$

The first term is the standard BCS expression, and describes coherent pairing occurring within a $(1 - x)$ fraction of the gapped part. The second term describes puddles that, although having a gap, are too small to exhibit phase coherence. We define w_{pair} as the total fraction of the system that can display pairing down to $T = 0$, and the coherently and incoherently paired fractions $w_{coh} = (1 - x) w_{pair}$ and $w_{inc} = x w_{pair}$. The latter term is necessary because the experimental spectra are gapped but display no coherence peaks when $V_g \ll 0$.²³ The gap is assumed to take the BCS expression

$$\Delta(T_c, T) = 1.76 T_c \tanh\left(\frac{\pi}{1.76} \sqrt{\frac{T_c - T}{T}}\right).$$

The value of N_0 is readily determined by the high-bias part of the spectra, while w , x , and the parameters of the distribution of critical temperatures, \bar{T}_c , γ , are used as fitting parameters.

At low temperature, accurate fits the spectra and of their evolution as a function of the gate voltage V_g were obtained.³⁰ Remarkably, the width of the distribution of critical temperatures, γ , turned out to be very weakly dependent of V_g , indicating that the distribution of T_c in the sample is essentially related to structural properties, like the local amount of disorder.

When fitting the temperature dependence of the spectra at fixed V_g , the attempt to make use of the same temperature-independent set of parameters, although capturing the main features of the spectra, yielded fits definitely less convincing than the fits at low temperature. However, releasing the severe constraint of temperature-independent parameters, very good fits are obtained by letting w and x vary, while the parameters of the distribution of critical temperatures, \bar{T}_c , γ are kept fixed. The variation of w and x with the temperature is more clearly understood when expressed through the quantities w_{coh} and w_{inc} defined above. It turns out that

the fraction of the sample occupied by the superconducting cluster increases with decreasing temperature, and saturates at low T , likely indicating that a sizable part of the metallic background is gradually driven superconducting by proximity effect.³⁰

VII. MULTIPLE QUANTUM CRITICAL BEHAVIOR IN INHOMOGENEOUS SUPERCONDUCTORS

The recent analysis of the quantum critical behavior that is observed when the superconducting phase is suppressed by means of a magnetic field perpendicular to the interface²¹ provided further support in favor of our scenario for inhomogeneous superconductivity at oxide interfaces. When the resistance R of LTO/STO, rescaled by a characteristic value \bar{R} , is plotted as a function of the variable $(B - \bar{B})/T^{1/z\nu}$, where \bar{B} is a characteristic magnetic field (see Fig. 8), z is the dynamical exponent (converting a critical length scale in a time scale), and ν is the critical exponent of the correlation length as a function of temperature, two quantum critical scaling regimes are found, in different temperature ranges. These two scaling regimes, separated by a crossover at intermediate temperatures, are in correspondence with two different values of the characteristic magnetic field $\bar{B} = B_{\times}, B_c$. The smaller field, B_{\times} , is related to the scaling at higher T , with $z\nu \approx \frac{2}{3}$, whereas the (slightly) larger field, B_c , corresponds to the scaling at lower T , with $z\nu \approx \frac{3}{2}$. Noticeably, the characteristic fields B_{\times} and B_c coalesce at low carrier density (i.e., low gate voltage V_g). When V_g is increased, B_{\times} saturates to a constant, whereas B_c closely tracks the superconducting critical temperature T_c (with a conversion factor of 1 T corresponding to 1 K).

A possible explanation for this multiple critical behavior relies on the assumption that superconductivity within an isolated puddle would be suppressed by the smaller critical field B_{\times} . However, the puddles are coupled, being embedded in a common metallic background.³¹ When inter-puddle coupling eventually intervenes, superconductivity is strengthened and survives up to the (slightly) larger critical field B_c . If we borrow the value of the dynamical exponent $z = 1$, which is commonly adopted in similar situations,³² the intra-puddle criticality is described by the XY model³³ in the clean limit, where $\nu \approx \frac{2}{3}$. However, with lowering the temperature, the coherence length increases, eventually exceeding the puddle size, and inter-puddle superconductivity establishes in the inhomogeneous landscape of puddles embedded in the metallic background. In this case, the exponent ν must obey the Harris criterion³⁴ for disordered systems, and indeed we find $\nu \approx \frac{3}{2} > 1$.

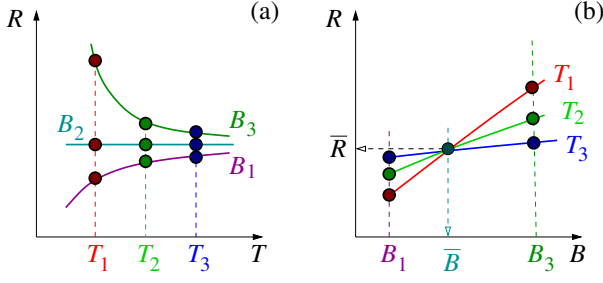


FIG. 8. Sketch of the procedure adopted to extract the quantum critical behavior when the superconducting phase is suppressed by means of a magnetic field perpendicular to the interface. (a) When the resistance R is plotted as a function of temperature T , three behaviors are observed over a certain temperature interval, exemplified by the curves corresponding to the three magnetic fields $B_1 < B_2 < B_3$: superconducting, critical, insulating. (b) To better identify the critical value of the magnetic field, B_c or B_\times , isotherms are plotted as a function of B , exemplified by the three curves corresponding to the temperatures $T_1 < T_2 < T_3$: the crossing point of the isotherms corresponds to \bar{B} (B_\times or B_c), and the corresponding characteristic value \bar{R} is obtained on the resistance axis.

VIII. MULTI-CARRIER BCS MODEL

According to the discussion developed so far, the inhomogeneous character of the 2DEG at the LXO/STO oxide interfaces induces a distribution $W(T_c)$ of local critical temperatures, its mean value \bar{T}_c depending on the overall carrier density (i.e., on V_g). This dependence is obtained fitting the resistance data in Fig. 5(a) within EMT, and sheds light on the intra-puddle pairing mechanism. As discussed in Sec. I, detailed magneto-transport measurements⁴ highlighted the coexistence of a sizable amount of low-mobility carriers and a smaller amount of high-mobility carriers in LTO/STO. Here, as well as in LAO/STO,³⁵ superconductivity seems definitely to develop as soon as the high-mobility carriers appear.

Accordingly, we proposed²² that superconducting pairing within the 2DEG formed at the oxide interface may be described by a multi-band^{36–40} BCS-like Hamiltonian

$$\mathcal{H}_{BCS} = \sum_{\mathbf{k}, \ell} \xi_{\mathbf{k}, \ell} \left(a_{\mathbf{k}, \ell, \uparrow}^\dagger a_{\mathbf{k}, \ell, \uparrow} + a_{\mathbf{k}, \ell, \downarrow}^\dagger a_{\mathbf{k}, \ell, \downarrow} \right) + \sum_{\substack{\mathbf{k}, \ell \\ \mathbf{k}', \ell'}}' \frac{g_{\ell \ell'}}{N} a_{\mathbf{k}, \ell, \uparrow}^\dagger a_{-\mathbf{k}, \ell, \downarrow}^\dagger a_{-\mathbf{k}', \ell', \downarrow} a_{\mathbf{k}', \ell', \uparrow} \quad (7)$$

where $a_{\mathbf{k}, \ell, \sigma}^\dagger$ ($a_{\mathbf{k}, \ell, \sigma}$) creates (annihilates) an electron with two-dimensional wave vector $\mathbf{k} = (k_x, k_y)$, parallel to the plane of the interface, and spin projection $\sigma = \uparrow, \downarrow$, belonging to the ℓ -th sub-band, with dispersion law

$$\xi_{\mathbf{k}, \ell} = \bar{\varepsilon}_\ell + \frac{\hbar^2 k_x^2}{2m_{\ell, x}} + \frac{\hbar^2 k_y^2}{2m_{\ell, y}} - \mu,$$

where $m_{\ell, x(y)}$ are the (possibly anisotropic) effective masses of the charge carriers and μ is the chemical potential, $g_{\ell \ell'}$ are the intraband (for $\ell = \ell'$) or interband

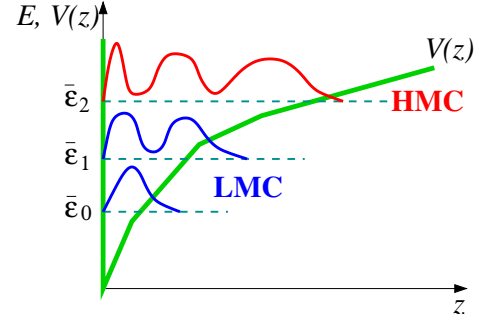


FIG. 9. Sketch of the quantized levels $\bar{\varepsilon}_\ell$ in the potential well $V(z)$ confining the 2DEG at the interface (z is the coordinate perpendicular to the interface), and of the corresponding carrier density distributions. The lower-lying levels, e.g., at energies $E = \bar{\varepsilon}_0, \bar{\varepsilon}_1$, accommodate the low-mobility carriers (LMC), whereas the topmost level, e.g., at $E = \bar{\varepsilon}_2$, hosts the high-mobility carriers (HMC).

(for $\ell \neq \ell'$) pairing amplitudes and N is the number of \mathbf{k} points within the first Brillouin zone. The sub-bands can originate, e.g., from the multiband structure of STO^{12,41} and/or from the quantum confinement within the self-consistent potential well at the interface.^{4,42} In our schematic description, we represent the whole set of low-lying bands with one sub-band ($\ell = 1$) accommodating the non superconducting low-mobility carriers, while the high-mobility carriers in the sub-band $\ell = 2$ are paired and give rise to a finite T_c (see Fig. 9, where a sub-band structure originating from the quantum confinement is sketched, readapted from a similar sketch in Ref. [22]).

Thus, according to our interpretation, the superconducting puddles are regions where the $\ell = 2$ sub-band is locally filled, whereas the (weakly localizing) metallic background corresponds to regions where the $\ell = 2$ sub-band is empty. The phenomenology of the superconducting phase at oxide interfaces is reproduced assuming that the pairing amplitudes are such that $g_{11} \ll (g_{12}, g_{21}) \ll g_{22}$. This condition is also consistent with the analysis of a two-band model in Ref. [43]. For simplicity, to reduce to a minimum the number of free parameters, in the following we assume that $g_{11} = g_{12} = g_{21} = 0$. According to the standard BCS approach, the pairing amplitudes are only effective in a window $|\xi_{\mathbf{k}, \ell}|, |\xi_{\mathbf{k}', \ell'}| \leq \hbar\omega_0$, where ω_0 is a characteristic cut-off frequency. The prime superscript attached to the last sum in Eq. (7) implies this restriction. We assume that the bottoms of the two sub-bands are well separated, $\bar{\varepsilon}_2 - \bar{\varepsilon}_1 \gg \hbar\omega_0$, and take henceforth $\bar{\varepsilon}_2 = 0$.

In principle, when deducing a BCS-like Hamiltonian, one should take care of vertex corrections (which are expected to be relevant when Migdal's condition is violated). However, the task of deducing a BCS-like Hamiltonian in a multi-band model, where electrons with large and small Fermi energy coexist, is overwhelmingly difficult. We rather take Eq. (7) as a phenomenological low-

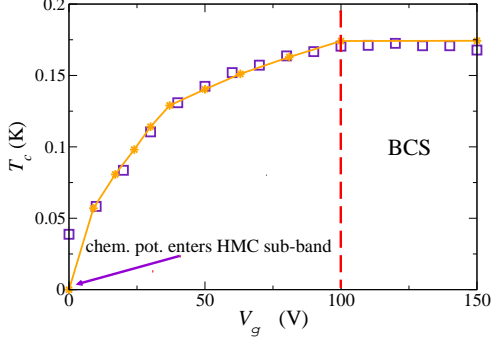


FIG. 10. Average critical temperature extracted from the EMT fit of the sheet resistance data (empty squares), and critical temperature of our BCS-like model (solid line with diamonds), as a function of V_g . T_c starts to rise when the chemical potential enters the HMC sub-band ($\mu = \bar{\varepsilon}_2$) and saturates to the standard BCS value when $\mu = \bar{\varepsilon}_2 + \hbar\omega_0$. The two regimes are separated by the dashed vertical line.

energy effective Hamiltonian, imagining that the various high-energy effects have been accounted for by a suitable dressing of the bare physical parameters. Thus, the identification of ω_0 with the characteristic frequency of the pairing mediator is expected to hold only indicatively.

For $\mu \leq 0$ the sub-band hosting the high-mobility carriers is empty and $T_c = 0$. For $0 < \mu < \hbar\omega_0$, pairing occurs at the critical temperature

$$T_c \approx 1.14 (\hbar\omega_0\mu)^{\frac{1}{2}} e^{-1/\lambda},$$

where $\lambda \equiv g_{22}N_0^{\text{HMC}}$ is the dimensionless superconducting coupling and N_0^{HMC} is the DOS of the sub-band filled by the high-mobility carriers. For $\mu \geq \hbar\omega_0$, T_c saturates to the standard BCS value

$$T_c^{\text{BCS}} \approx 1.14 \hbar\omega_0 e^{-1/\lambda}.$$

The previous results can be cast into a single expression

$$T_c(\mu) = T_c^{\text{BCS}} \vartheta(\mu) \min\left(\sqrt{\frac{\mu}{\hbar\omega_0}}, 1\right). \quad (8)$$

Remarkably, the amplitude $\Delta\mu$ of the interval in correspondence of which T_c is an increasing function of μ provides a direct measure of the cut-off energy scale, $\hbar\omega_0 = \Delta\mu$, which, with the caveat recalled above, we interpret as a possibly crude estimate of the characteristic energy scale of the pairing mediator.

The fit of the curve $\bar{T}_c(V_g)$, extracted from the experimental data in Fig. 5(a) within EMT, with the curve $T_c(\mu)$ in Eq. (8), exploiting the approximately linear relation between V_g and μ ,⁴ yields the result illustrated in Fig. 10 (orange line with diamonds and empty squares, respectively). Fig. 10 is inspired to a similar figure of Ref. [22], redrawn here in a modified fashion, to make explicit contact with the overview contained in this piece

of work. The various band masses are taken all equal to 0.7 electron masses, corresponding to a scenario where the sub-band structure originates from quantum confinement of the lowest t_{2g} band of bulk STO near the interface. We then obtain the dimensionless coupling constant $\lambda \approx 0.125$ (therefore, consistent with our assumption that the system falls in the weak coupling regime) and a cut-off energy scale $\hbar\omega_0 \approx 23$ meV, which is compatible with a typical phonon energy in STO.²⁹

IX. CONCLUDING REMARKS

In conclusion, we first analyzed magneto-transport experiments in LTO/STO oxide interfaces⁴ within a multi-carrier EMT model, confirming the occurrence of two kind of carriers, with high and low mobility, within an inhomogeneous landscape. We proposed that the system consists of regions with higher carrier density, where both carrier coexist, and regions with lower carrier density, where only the low-mobility carriers are present. We also confirm that the high-mobility carriers have a lower density than the low-mobility ones. The mobilities of the two species turn out to be almost independent of the gate voltage. Thus, the enhancement of conductivity observed around $V_g = 0$ V and the change in the slope of the Hall resistance at high magnetic field occur because a finite fraction w of regions with higher carrier density, hosting high-mobility carriers, appears around this gate voltage.

We then described superconductivity in LAO/STO and LTO/STO within a scenario in which superconducting puddles (the regions with coexisting high and low-mobility carriers) are embedded in a metallic background (the regions with low-mobility carriers only), and form a percolating network. In this framework, the sheet resistance of LTO/STO interfaces is very well described by EMT or by a RRN for an inhomogeneous 2DEG with a substantial filamentary character. Fitting the experiments, we were able to extract the random distribution of T_c at various V_g (i.e., various carrier densities). A similar approach was adopted to fit the microscopically averaged superfluid stiffness¹⁰ and the pseudogap in tunneling spectra²³ of LAO/STO. In particular, we showed that our model accounts well for the metal-insulator-superconductor tunneling spectra measured in LAO/STO, and allows us to draw the conclusion that the fraction of the sample occupied by the superconducting puddles increases when the temperature is reduced, and saturates at low temperature, likely indicating that also a sizable fraction of the metallic background gradually becomes superconducting by proximity effect.

Assuming an effective two-band model with superconductivity triggered by the presence of few high-mobility carriers, locally filling the highest-energy band, we account for the density dependence of the intra-puddle T_c within a simple BCS weak coupling scheme. As an important by-product, we find that the range of variation in V_g of the (average) intra-puddle T_c is directly related

(via the chemical potential μ) to the cut-off energy scale $\hbar\omega_0$. Taking this value as a crude estimate of the typical energy scale of the pairing mediator, we find that this is compatible with phonon-mediated superconductivity.

Although this was not the main focus of the present piece of work, few words are now in order to discuss the origin of electron inhomogeneity at LXO/STO interfaces. Extrinsic mechanisms,⁴⁴ like impurities and growth defects are always accountable of rendering an interface inhomogeneous. However, experimental data show that inhomogeneity is never reduced below a still sizable extent, even in the best samples. Furthermore, the observation of negative electron compressibility in a low-filling regime⁴⁵ suggests that intrinsic mechanisms (e.g., in the form of effective electron-electron attractions) are present, which may render the 2DEG formed at the LXO/STO interface inhomogeneous by phase separation, even in a perfectly clean and expectedly homogeneous system. These facts led us to look for intrinsic mechanisms of inhomogeneity. A possible intrinsic mechanism for the formation of an inhomogeneous 2DEG was proposed,^{12,41} that relies on the strong density dependent RSOC inferred at these interfaces,¹¹ and yields a non-rigid band structure, with the possibility that the chemical potential of the carriers is a non-monotonic function of the carrier density for reasonable values of the model parameters, giving rise to a thermodynamic instability. The resulting

RSOC-driven electronic phase separation provides a natural framework for the occurrence of regions with higher and lower carrier density (the superconducting puddles and the metallic background, respectively), accounting for the inhomogeneous character of the superconducting phase at oxide interfaces. Of course, whenever electronic phase separation comes about, one should worry about the Coulomb energy cost to be paid for the segregation of charge carriers. Thanks to the large dielectric constant of STO, we showed⁴¹ that the size of the domains can grow as large as several tens of nanometers. An alternative route to intrinsic inhomogeneity might be provided by the pronounced density dependence of the self-consistent potential well $V(z)$ confining the 2DEG at the interface (see Fig. 9). Calculations within a Schrödinger-Poisson self-consistent scheme⁴² show indeed that also this mechanism is apt to yield a non-monotonic chemical potential, again resulting in electronic phase separation.

Acknowledgments. S.C. and M.G. acknowledge financial support from “AWARDS Projects” of the University of Rome Sapienza, n. C26H13KZS9. This work has been supported by the Region Île-de-France in the framework of CNano IdF and Sesame programs, and by the DGA PhD program.

-
- ¹ N. Reyren, S. Thiel, A. D. Caviglia, L. Fitting Kourkoutis, G. Hammerl, C. Richter, C. W. Schneider, T. Kopp, A.-S. Retschi, D. Jaccard, M. Gabay, D. A. Muller, J.-M. Triscone, and J. Mannhart, *Science* **317**, 1196 (2007).
 - ² A. Caviglia, S. Gariglio, N. Reyren, D. Jaccard, T. Schneider, M. Gabay, S. Thiel, G. Hammerl, J. Mannhart, and J.-M. Triscone, *Nature (London)* **456**, 624 (2008).
 - ³ J. Biscaras, N. Bergeal, A. Kushwaha, T. Wolf, A. Rastogi, R. C. Budhani, and J. Lesueur, *Nat. Commun.* **1**, 89 (2010).
 - ⁴ J. Biscaras, N. Bergeal, S. Hurand, C. Grossetête, A. Rastogi, R. C. Budhani, D. LeBoeuf, C. Proust, and J. Lesueur, *Phys. Rev. Lett.* **108**, 247004 (2012).
 - ⁵ Ariando, X. Wang, G. Baskaran, Z. Q. Liu, J. Huijben, J. B. Yi, A. Annadi, A. Roy Barman, A. Rusydi, S. Dhar, Y. P. Feng, J. Ding, H. Hilgenkamp, and T. Venkatesan, *Nat. Commun.* **2**, 188 (2011).
 - ⁶ Lu Li, C. Richter, J. Mannhart, and R. C. Ashoori, *Nat. Phys.* **7**, 762 (2011).
 - ⁷ J. A. Bert, B. Kalisky, C. Bell, M. Kim, Y. Hikita, H. Y. Hwang, and K. A. Moler, *Nat. Phys.* **7**, 767 (2011).
 - ⁸ D. A. Dikin, M. Mehta, C. W. Bark, C. M. Folkman, C. B. Eom, and V. Chandrasekhar, *Phys. Rev. Lett.* **107**, 056802 (2011).
 - ⁹ M. M. Mehta, D. A. Dikin, C. W. Bark, S. Ryu, C. M. Folkman, C. B. Eom, and V. Chandrasekhar, *Nat. Commun.* **3**, 955 (2012).
 - ¹⁰ J. A. Bert, K. C. Nowack, B. Kalisky, H. Noad, J. R. Kirtley, C. Bell, H. K. Sato, M. Hosoda, Y. Hikita, H. Y. Hwang, K. A. Moler, *Phys. Rev. B* **86**, 060503(R) (2012).
 - ¹¹ A. D. Caviglia, M. Gabay, S. Gariglio, N. Reyren, C. Cancellieri, and J.-M. Triscone, *Phys. Rev. Lett.* **104**, 126803 (2010).
 - ¹² S. Caprara, F. Peronaci, and M. Grilli, *Phys. Rev. Lett.* **109**, 196401 (2012).
 - ¹³ Y. A. Bychkov and E. I. Rashba, *J. Phys. C* **17**, 6039 (1984).
 - ¹⁴ C. Bell, S. Harashima, Y. Kozuka, M. Kim, B. G. Kim, Y. Hikita, and H. Y. Hwang, *Phys. Rev. Lett.* **103**, 226802 (2009).
 - ¹⁵ S. Caprara, M. Grilli, L. Benfatto, and C. Castellani, *Phys. Rev. B* **84**, 014514 (2011).
 - ¹⁶ D. Bucheli, S. Caprara, C. Castellani, and M. Grilli, *New J. Phys.* **15**, 023014 (2013).
 - ¹⁷ Z. Ristic, R. Di Capua, G. M. De Luca, F. Chiarella, G. Ghiringhelli, J. C. Cezar, N. B. Brookes, C. Richter, J. Mannhart and M. Salluzzo, *Europhys. Lett.* **93**, 17004 (2011).
 - ¹⁸ F. Bi, M. Huang, C. W. Bark, S. Ryu, S. Lee, C.-B. Eom, P. Irvin, and J. Levy, arXiv:1302.0204.
 - ¹⁹ B. Kalisky, private communication and APS March Meeting 2013.
 - ²⁰ S. Ilani, private communication.
 - ²¹ J. Biscaras, N. Bergeal, S. Hurand, C. Feuillet-Palma, A. Rastogi, R. C. Budhani, M. Grilli, S. Caprara, and J. Lesueur, *Nat. Mater.* **12**, 542 (2013).
 - ²² S. Caprara, J. Biscaras, N. Bergeal, D. Bucheli, S. Hurand, C. Feuillet-Palma, A. Rastogi, R. C. Budhani, J. Lesueur, and M. Grilli, *Phys. Rev. B* **88**, 020504(R) (2013).
 - ²³ C. Richter, H. Boschker, W. Dietsche, E. Fillis-Tsirakis, R.

- Jany, F. Loder, L. F. Kourkoutis, D. A. Muller, J. R. Kirtley, C. W. Schneider, and J. Mannhart, *Nature* (London) **502**, 528 (2013).
- ²⁴ V. E. Arkhincheev, *JETP* **91**, 407 (2000).
- ²⁵ Proximity effects in inhomogeneous superconductors are discussed in detail, e.g., in Yu. N. Ovchinnikov, S. A. Wolf, and V. Z. Kresin, *Phys. Rev. B* **63**, 064524 (2001); V. Z. Kresin, Yu. N. Ovchinnikov, and S. A. Wolf, *Phys. Rep.* **431**, 231 (2006).
- ²⁶ D. Stornaiuolo, S. Gariglio, N. J. G. Couto, A. Fête, A. D. Caviglia, G. Seyfarth, D. Jaccard, A. F. Morpurgo, and J.-M. Triscone, *Appl. Phys. Lett.* **101**, 222601 (2012).
- ²⁷ D. Stauffer and A. Aharony, *Introduction to Percolation Theory*, 2nd ed. (Taylor and Francis, London, 1994).
- ²⁸ R. A. Muniz and I. Martin, *Phys. Rev. Lett.* **107**, 127001 (2011).
- ²⁹ C. S. Koonce, M. L. Cohen, J. F. Schooley, W. R. Hosler, and E. R. Pfeiffer, *Phys. Rev.* **163**, 380 (1967).
- ³⁰ D. Bucheli, S. Caprara, and M. Grilli, arXiv:1405.4666.
- ³¹ B. Spivak, P. Oreto, and S. Kivelson, *Phys. Rev. B* **77**, 214523 (2008).
- ³² S. L. Sondhi, S. M. Girvin, J. P. Carini, and D. Shahar, *Rev. Mod. Phys.* **69**, 315 (1997); M. P. A. Fisher, *Phys. Rev. Lett.* **65**, 923 (1990).
- ³³ D. Jasnow and M. Wortis, *Phys. Rev.* **176**, 739 (1968); K. Wilson and M. Fisher, *Phys. Rev. Lett.* **28**, 240 (1972); Y. H. Li, and S. Teitel, *Phys. Rev. B* **40**, 9122 (1989); J. Kisker and H. Rieger, *Phys. Rev. B* **55**, R11981 (1997).
- ³⁴ H. B. Harris, *J. Phys. C* **7**, 1671 (1974).
- ³⁵ D. Rakhmilevitch, I. Neder, M. Ben Shalom, A. Tsukernik, M. Karpovski, Y. Dagan, and A. Palevski, arXiv:1301.1055v1.
- ³⁶ M. Salluzzo, J. C. Cezar, N. B. Brookes, V. Bisogni, G. M. De Luca, C. Richter, S. Thiel, J. Mannhart, M. Huijben, A. Brinkman, G. Rijnders, and G. Ghiringhelli, *Phys. Rev. Lett.* **102**, 166804 (2009).
- ³⁷ A. Joshua, S. Pecker, J. Ruhman, E. Altman and S. Ilani, *Nat. Commun.* **3**, 1129 (2012).
- ³⁸ P. Delugas, A. Filippetti, V. Fiorentini, D. I. Bilc, D. Fontaine, and P. Ghosez, *Phys. Rev. Lett.* **106**, 166807 (2011).
- ³⁹ Z. Zhong, A. Töth, and K. Held, *Phys. Rev. B* **87**, 161102(R) (2013).
- ⁴⁰ D. Innocenti, N. Poccia, A. Ricci, A. Valletta, S. Caprara, A. Perali, and A. Bianconi, *Phys. Rev. B* **82**, 184528 (2010); D. Innocenti, S. Caprara, N. Poccia, A. Ricci, A. Valletta, and A. Bianconi, *Supercond. Sci. Technol.* **24**, 015012 (2011).
- ⁴¹ D. Bucheli, M. Grilli, F. Peronaci, G. Seibold, and S. Caprara, *Phys. Rev. B* **89**, 195448 (2014).
- ⁴² N. Scopigno, D. Bucheli, S. Caprara, and M. Grilli, in preparation.
- ⁴³ R. M. Fernandes, J. T. Haraldsen, P. Wölfe, and A. V. Balatsky, *Phys. Rev. B* **87**, 014510 (2013).
- ⁴⁴ N. C. Bristowe, T. Fix, M. G. Blamire, P. B. Littlewood, and E. Artacho, *Phys. Rev. Lett.* **108**, 166802 (2012).
- ⁴⁵ Lu Li, C. Richter, S. Paetel, T. Kopp, J. Mannhart, and R. C. Ashoori, *Science* **332**, 825 (2011).